

MeV femtosecond electron pulses from direct-field acceleration in low density atomic gases

Charles Varin¹, Vincent Marceau², Pascal Hogan-Lamarre², Thomas Fennel³, Michel Piché², and Thomas Brabec¹

1 Center for Research in Photonics, University of Ottawa, Ottawa (ON) K1N 6N5, Canada

2 Centre d'Optique, Photonique et Laser, Université Laval, Québec (QC) G1V 0A6, Canada

3 Institut für Physik, Universität Rostock, 18051 Rostock, Germany

Abstract. Using three-dimensional particle-in-cell simulations, we show that few-MeV electrons can be produced by focusing tightly few-cycle radially-polarized laser pulses in a low-density atomic gas. In particular, it is observed that for the few-TW laser power needed to reach relativistic electron energies, longitudinal attosecond microbunching occurs naturally, resulting in femtosecond structures with high-contrast attosecond density modulations. The three-dimensional particle-in-cell simulations show that in the relativistic regime the leading pulse of these attosecond substructures survives to propagation over extended distances, suggesting that it could be delivered to a distant target, with the help of a properly designed transport beamline.

PACS numbers: 41.75.Jv, 52.38.-r, 61.05.J

Keywords: *laser-driven electron acceleration, radially polarized laser beams, ultrashort electron pulse*

1. Introduction

Optical electron acceleration is an important application of high-power lasers, in particular for the development of new electron and radiation sources for probing ultrafast structural dynamics in matter [1, 2]. So far, research has mainly focused on the lower and upper limits of the energy spectrum: subrelativistic energies for ultrafast electron diffraction (UED) [3–9] and ultrarelativistic energies for the development of compact radiation sources [10–13]. In comparison, little attention has been paid to optical electron acceleration in the few-MeV range.

MeV electrons are of interest for relativistic time-resolved electron diffraction [14, 15], as well as for controlled injection in staged laser wakefield accelerators [16, 17] and dielectric acceleration structures [7, 18, 19] that in turn can drive table-top synchrotron radiation sources [10–13]. In particular for diffraction with ultrashort electron pulses, the suppression of space-charge effects at relativistic energies allows packing more electrons per bunch while maintaining ultrashort duration at a distant target. This enables single-shot studies of ultrafast structural processes that are out of reach of conventional (non-relativistic) UED [20].

There actually exist ultrafast sources of MeV electrons. For example, radio frequency (rf) photoguns can produce few-MeV pulses with 100-fs duration [2, 15, 21] and there are proposals to obtain even shorter durations (~ 10 fs) with an rf compressor [22]. However, using a laser-based acceleration mechanism has the following potential advantages: (i) the short wavelength of the accelerating field may lead to electron bunches with initial durations of the order of 10 fs or less; (ii) the intrinsic synchronization between the laser and electron pulses is essentially jitter free; (iii) compared with nanoclusters and thin

film targets, optimization using a gas medium does not require sub-wavelength alignment of the target position; (iv) using a gas medium, the target is self-regenerating and can thus be used for experiments at high repetition rates. Breakthrough laser-driven plasma acceleration experiments demonstrated the production of presumably sub-100-fs electron pulses in the tens-of-MeV range [23] and a method to obtain 15-fs pulses in the 5–10 MeV range was proposed [24].

In this article, we show how ultrashort MeV electron pulses can be produced by tightly focusing few-TW radially-polarized femtosecond laser pulses (RPFLPs) in a low-density gas. We investigate the laser-gas interaction and electron acceleration in a configuration similar to the experiment reported by Payeur *et al.* [5] with three-dimensional particle-in-cell (3DPIC) simulations. In particular, we observed attosecond microbunching within a longer femtosecond structure for a laser power in the few-TW range. This is about two orders of magnitude lower than previously demonstrated for direct-field electron acceleration [25, 26]. We show that some of these microbunches survive to propagation in space, suggesting that the proposed method could enable the delivery of sub-femtosecond electron pulses to a distant target with the current laser and beamline technology.

This paper is divided as follows. First in Sec. 2, we present our 3DPIC modelling approach to relativistic RPFLP-gas interaction. The analysis includes an exact analytical solution to Maxwell's equations for the spatiotemporal distribution of tightly-focused RPFLPs and the complete ionization and plasmas dynamics starting from a neutral atomic gas. In Sec. 3, we explain why MeV electron energies and attosecond bunching are expected in the few-TW regime under tight focusing conditions. Analytical predictions are confirmed with 3DPIC simulations. Fi-

nally in Sec. 4, we analyze the propagation of the electron pulses and explain how the electron distributions could be filtered to isolate the leading substructure.

2. Relativistic laser-gas interaction model

To simulate the complete ultrafast and ultra-intense RPFLP-gas interaction, we performed 3DPIC simulations with full atomic ionization and charge dynamics. In particular, we used a customized version of the EPOCH PIC code [27], where the electromagnetic field of the RPFLP is introduced using the FDTD scattered-field formulation [28]. This approach allows us to provide the most accurate description of tightly-focused RPFLPs *via* the analytical vacuum-field solution.

For the vacuum field representing the incident RPFLP, we use an exact closed-form spatiotemporal formulation given by the following expressions in cylindrical coordinates, with $\mathbf{r} = (r, \theta, z)$ [29, 30]:

$$E_r(\mathbf{r}, t) = \frac{3E_0 \sin 2\tilde{\Theta}}{2\tilde{R}} \left(\frac{G_-^{(0)}}{\tilde{R}^2} + \frac{G_+^{(1)}}{c\tilde{R}} + \frac{G_-^{(2)}}{3c^2} \right), \quad (1)$$

$$E_z(\mathbf{r}, t) = \frac{E_0}{\tilde{R}} \left[\frac{(3 \cos^2 \tilde{\Theta} - 1)}{\tilde{R}} \left(\frac{G_-^{(0)}}{\tilde{R}} + \frac{G_+^{(1)}}{c} \right) - \frac{\sin^2 \tilde{\Theta}}{c^2} G_-^{(2)} \right], \quad (2)$$

$$B_\phi(\mathbf{r}, t) = \frac{E_0 \sin \tilde{\Theta}}{c\tilde{R}} \left(\frac{G_-^{(1)}}{c\tilde{R}} + \frac{G_+^{(2)}}{c^2} \right). \quad (3)$$

The physical fields \mathbf{E} and \mathbf{B} are obtained by taking the real part of the corresponding expressions. E_0 is the amplitude of the transverse electric field component and c is the speed of light *in vacuo*. The complex variables are defined as follows: $\tilde{R} = [r^2 + (z + ja)^2]^{1/2}$, $\cos \tilde{\Theta} = (z + ja)/\tilde{R}$, and $G_\pm^{(n)} = \partial_t^n [f(\tilde{t}_-) \pm f(\tilde{t}_+)]$ with $\tilde{t}_\pm = t \pm \tilde{R}/c + ja/c$. The confocal parameter a is associated with the Rayleigh range z_R by $k_0 z_R = \sqrt{1 + (k_0 a)^2} - 1$ [31], where $k_0 = 2\pi/\lambda_0$, λ_0 being the central wavelength of the laser.

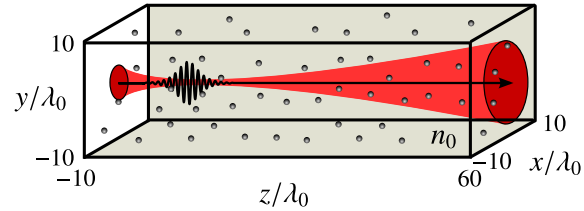


Figure 1. Schematic representation of the laser-gas interaction model analyzed with 3D particle-in-cell simulations (3DPIC).

A Poisson-like pulse spectrum [32] was assumed, with the corresponding temporal form $f(t) = e^{-j\phi_0} (1 - j\omega_0 t/s)^{-(s+1)}$, where ϕ_0 is the constant pulse phase and $\omega_0 = ck_0$ the central angular frequency of the pulse spectrum. The parameter s is a positive constant related to the pulse duration. In the limit where $s \gg 1$, the usual carrier-envelope temporal function $f(t) \simeq e^{-t^2/T^2} e^{j(\omega_0 t - \phi_0)}$ is recovered, with $T \simeq \sqrt{2s}/\omega_0$. From an experimental point of view, the fields given by Eqs. (1)–(3) can be produced by focusing a collimated radially-polarized input beam with a parabolic mirror of large numerical aperture [5, 33].

Typical numerical simulations are done with a cartesian mesh of size $600 \times 600 \times 2100$ with $N_\lambda = 30$ grid points per wavelength, spanning the region $x, y \in [-10\lambda_0, 10\lambda_0]$ and $z \in [-10\lambda_0, 60\lambda_0]$. We have observed that increasing the grid resolution to $N_\lambda = 40$ did not change the results significantly. At $t = 0$, the laser pulse is outside the simulation domain and the gas is represented by neutral atoms randomly distributed in the simulation volume and modeled by some 10^8 particle markers. A schematic illustration of the simulation setup is given in Fig. 1.

Throughout the simulations, multiphoton, tunnel, and barrier-suppression ionization were taken into account, as well as the motion of the ions and its effect on the electron trajectories (implementation details are found in [34]). Due to

the low density of the ionized medium, collisions and electron impact ionization were neglected.

We recall that in analogy to the standard normalized transverse vector potential parameter $a_0 = e|E|/m_e c \omega_0$ [35], when considering an RPFLP it is useful to introduce a normalized longitudinal parameter $a_z = e|E_z|_{peak}/m_e c \omega_0$ [36], where $|E_z|_{peak}$ is the amplitude of the longitudinal electric field component given at Eq. (2). When $a_z \geq 1$, the motion of a free electron in the longitudinal electric field of a RPFLP is relativistic.

3. Direct-field electron acceleration and attosecond bunching with RPFLPs tightly focused in a low-density gas

In previous publications [8, 9], it was shown that femtosecond few-hundred-keV electron pulses with percent-level energy spread can be produced by tightly focusing few-mJ RPFLPs in an hydrogen gas whose density is in the 10^{22} m^{-3} range. In particular, it was demonstrated that the laser pulse parameters and gas density can be optimized to cover the 100 – 300 keV energy window that characterizes ultrafast electron diffraction imaging experiments [20].

At a dominant wavelength of $\lambda_0 = 800 \text{ nm}$, typical pulse parameters were $k_0 a = 20$, $s = 70$, and $P = 300 \text{ GW}$, corresponding to a few-mJ 8-fs full width at half maximum (FWHM) pulse focused to a $2\lambda_0$ spot diameter. These parameters, defined by an extensive set of optimization calculations [9], were found to offer a good compromise between transverse and longitudinal effects, with a positive impact on electron energy, bunch charge, divergence, and energy spread.

In the regime explored in [8, 9], the normalized longitudinal parameter a_z is slightly larger than unity. In such conditions, the longitudinal electric field is too weak to induce a strong longitudinal compression and attosecond bunching

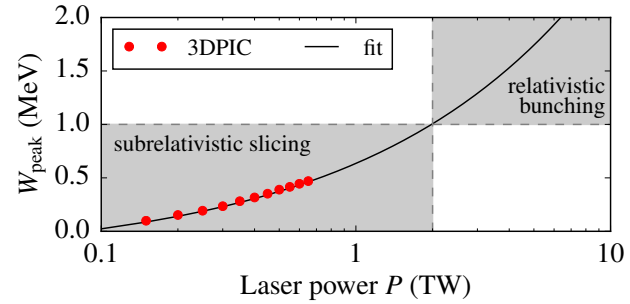


Figure 2. Analysis of electron acceleration in tightly-focused RPFLP as a function of the laser power. Red dots (•) are 3DPIC data points from Fig. 5(a) of [9], while the solid black line (—) is a fit of the form $a + b \sqrt{P}$ (see also [37]). We identified in gray two different ultrashort electron pulse regimes: the subrelativistic slicing regime, where only a thin disk of electron is accelerated (see, e.g., [8]), and the relativistic bunching regime, where electrons are compressed axially into attosecond pulses (see, e.g., [36]).

(see, e.g., explanations in [36]). Instead, the ultrashort electron pulse duration is due to the acceleration of a thin disk of electrons located in a very restricted region of the infinite gas target [8]. Electrons outside this thin disk region are either deflected away from the optical axis or gain little energy from the laser field. This results effectively in electron pulses with initial sub-femtosecond duration. However, the duration of these sub-relativistic pulses increases rapidly as they propagate due to electrostatic repulsion and the finite initial energy spread.

To predict the conditions to reach the relativistic regime—where longitudinal compression would become important—we fitted results from [9] for the electron energy as a function of the power P of the incident laser pulse. We used a \sqrt{P} scaling law that characterizes direct-field acceleration (see, e.g., [37]). Results are shown in Fig. 2. Conclusions are: (1) average MeV energies should be reached when $P > 2 \text{ TW}$ and (2) for strong focusing conditions ($z_R \sim \lambda_0$), in the few-TW power range, the longitudinal electric field has a super-relativistic strength ($a_z^2 \gg 1$). According to the 1D longitudinal direct-field

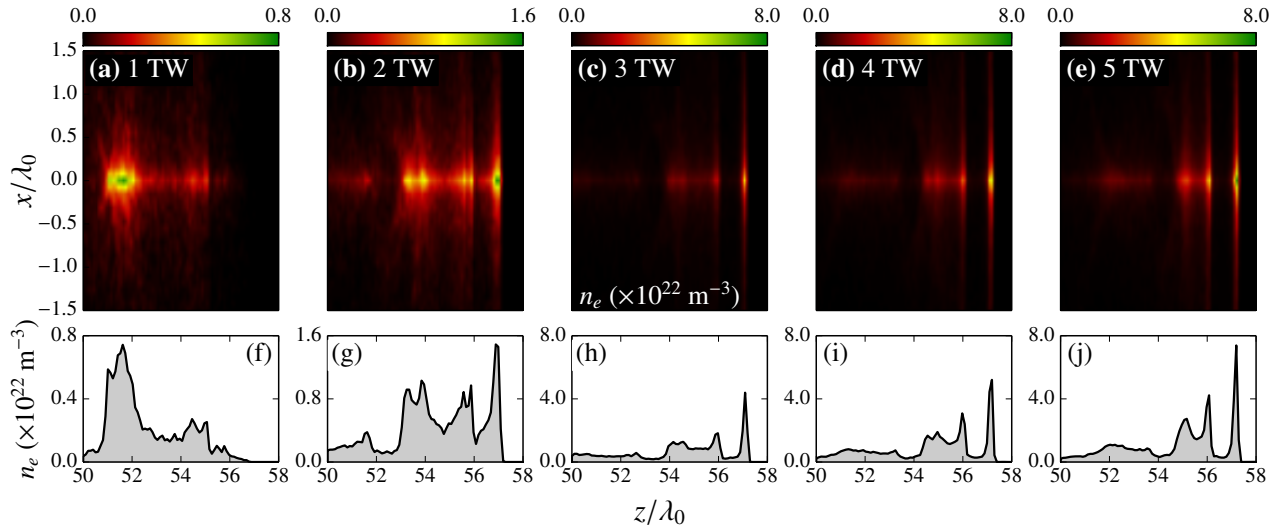


Figure 3. 3DPIC analysis of the transition to the relativistic regime of direct-field electron acceleration by RPFLPs tightly focused in a low density helium gas ($k_0a = 20$, $s = 70$, $\phi_0 = \pi$, and $n_{\text{He}} = 10^{22} \text{ m}^{-3}$). (a)-(e) are 2D cuts of the 3D electron density structures away from the RPFLP focus along the z coordinate for different values of the laser power. (f)-(j) are 1D cuts at $x = 0$ of the corresponding top graphs. Looking at (a) to (c) and (f) to (h), one sees clearly the transition from the subrelativistic slicing regime to the relativistic attosecond bunching regime, where the density distribution exhibits a sharp modulation at the leading edge due to sub-cycle compression of the accelerated electrons. Below the relativistic compression threshold in (a)-(b), the electron density has a peak value less than the initial bound-electron density ($n_e = 2n_{\text{He}}$). However in (c)-(e) above threshold, the compressed electron densities have peak values greater than $2n_{\text{He}}$. Still in (c)-(e), it is observed that the peak density increases with the laser power, without important changes in the macrobunches structure. Ultimately in (e), the peak charge density exceeds that of (a) by an order of magnitude. Total charge in the 3D macrobunches was found to be approximately (a) 1 fC, (b) 2 fC, (c) 3 fC, (d) 4 fC, and (e) 5 fC. Charge in the leading bunch is about (b) 0.35 fC, (c) 0.67 fC, (d) 0.85 fC, and (e) 1.05 fC.

acceleration model [36], longitudinal attosecond bunching should then occur naturally.

To validate our predictions, we simulated electron acceleration in helium with the 3DPIC method discussed in Sec. 2. For direct comparison with the results obtained in the subrelativistic electron regime [8,9], we used the following pulse parameters: $k_0a = 20$, $s = 70$, and $\phi_0 = \pi$, with a laser power in the 1-5 TW range.

Results from the 3DPIC analysis are shown in Fig. 3. They reveal that a high-contrast attosecond modulation of a longer femtosecond electron pulse structure is effectively produced when the laser power is in the few TW range. This corresponds to sub-100-mJ laser pulse energy. We recall that previous demonstrations assumed Joules (few-cycle pulses, 100 TW) or more to

produce similar attosecond bunching [25, 26]. In these studies, nanoclusters were considered to restrict the initial volume occupied by the free electrons. Here, the attosecond electron microbunches are produced in an infinite gas target. This configuration is much simpler, as it does not require particular target alignment.

From the spectra given in Fig. 4, it is evident that the femtosecond electron structures shown in Fig. 3 are composed of electrons with a broad distribution of energy. They are thus unlikely to remain together over an extended period of time. However, the spectral analysis of particular substructures (not shown) suggest that these complex femtosecond pulses are effectively composed of individual subpulses. We analyze this aspect in the following section by looking at

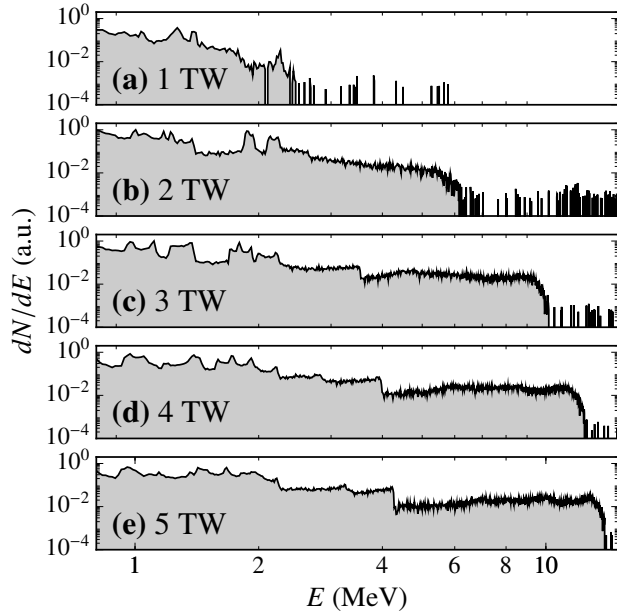


Figure 4. The broad energy spectra associated with the femtosecond electron structures shown in Fig. 3.

the evolution of the macrobunches over time, e.g., during propagation to a distant target.

4. Analysis of the propagation to a distant target

Electrostatic repulsion and electron momentum dispersion cause the spatio-temporal broadening of an electron pulse in time (see, e.g., [38]). For ultrashort pulses, the effect is predominantly longitudinal, causing the increase of the duration as the bunch travels in space [39]. In case of a broad spectrum, like shown in Fig. 4, an electron pulse might literally break up before it can be delivered to a distant target, e.g., where it would interact with a sample to produce a useful diffraction pattern.

We analyzed the propagation of the electron pulse structures shown in Fig. 3 with 3DPIC by using the moving window technique, where the numerical mesh is translated at the speed of light to follow the electron pulses as they move. The maximum physical time and distance that can be

simulated depend on the computational resources available, essentially. With the parameters given in Sec. 2, but where $x, y \in [-5\lambda_0, 5\lambda_0]$ to reduce the computational load, simulating a 700-fs propagation takes about 40 hours on a supercomputer using some 128 processes. It corresponds to a distance of 0.2 mm away from the RPFLP focus, comparable to the longitudinal distances reached in similar PIC studies [24].

The results given in Fig. 5 show that at the relativistic threshold (2 TW), the initial density modulations are lost during propagation. However, above threshold (> 2 TW) the leading substructure survives. For the electrons accelerated by the 5-TW RPFLP, it even maintained a sub-femtosecond duration up to the propagated distance that we could simulate. In comparison, a subrelativistic bunch with a comparable initial duration and charge would have a duration in the tens-of-fs range (see, e.g., [9]).

The macrobunches produced in the longitudinal compression regime share these common features: a fast and sharp leading structure followed by a slower trailing complex. We have observed that by applying a high-pass energy filter, the leading pulse structure is isolated. Conceptually, such an energy filter is implemented by deflecting the electrons with a magnetic field and putting an obstacle in the path of the electrons with energies that need to be removed. This approach was demonstrated in the femtosecond regime by filtering the electron energy directly into a magnetic compression device [40]. In principle, the same technique can be used for attosecond electron pulses (see, e.g., [41]), although the efficiency of the approach in the multi-electron regime still needs to be demonstrated.

To simulate the impact of an energy filter, we applied a numerical energy cutoff to the bunch structure shown in Fig. 5(h), by rejecting all the electrons with an energy less than 3 MeV. The resulting bunch, shown in Fig. 6, has a 480-as

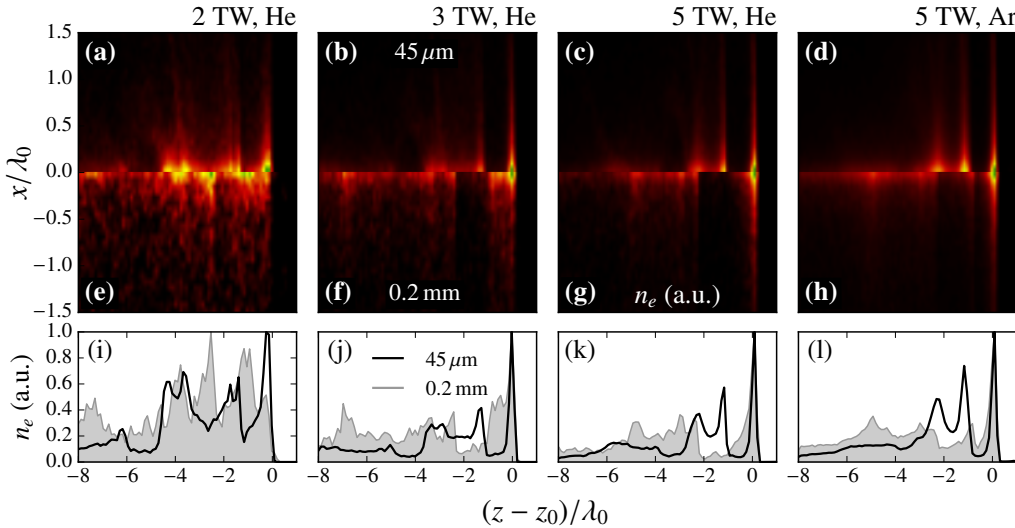


Figure 5. 3DPIC analysis of the evolution of the relativistic electron macrobunches produced by a few-TW RPFLP tightly focused in a low density gas ($k_0a = 20$, $s = 70$, $\phi_0 = \pi$, and $n = 10^{22} \text{ m}^{-3}$). Color plots show 2D cuts of the 3D electron density distributions n_e away from the optical focus. (a)-(d) $z_0 = 45 \mu\text{m}$ and (e)-(h) $z_0 = 0.2 \text{ mm}$. (i)-(l) are 1D cuts at $x = 0$ of the same distributions: $45 \mu\text{m}$ as a solid black line and 0.2 mm as a gray area. All distributions were normalized for direct comparison. For $P = 2 \text{ TW}$ [(a), (e), and (i)], the structure spreads out and the initial longitudinal modulation disappears. For $P = 3 \text{ TW}$ [(b), (f), and (j)], the leading attosecond pulse is still apparent after propagation, but with a much broader base. For $P = 5 \text{ TW}$ [(c), (g), and (k)], the trailing structure of slow electrons spreads out, but broadening of the leading pulse base is limited. For $P = 5 \text{ TW}$, comparison between simulations with helium [(c), (g), and (k)] and argon [(d), (h), and (l)] shows that the formation of the leading bunch does not depend on a specific gas element and that electrostatic repulsion between the electrons has a negligible influence, as expected in the relativistic regime. The initial bunch charge in (d) was about 37 fC, 7 times higher than that of the bunch shown in Fig. 3(e), with a proportional computational load.

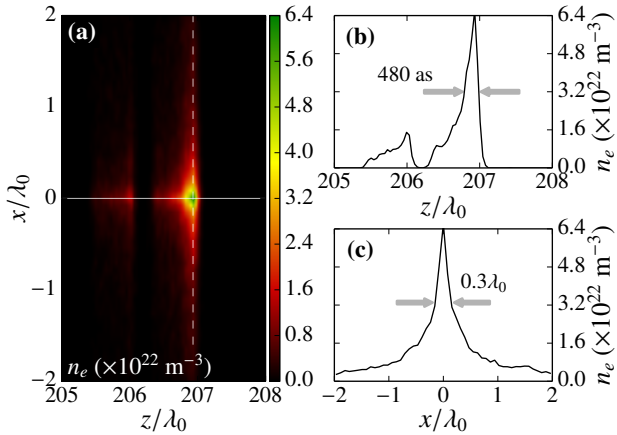


Figure 6. Spatio-temporal distribution of the macrobunch of Fig. 5(h) after electrons with energy less than 3 MeV where filtered out. Even if the bunch is effectively 0.2 mm away from the optical focus, the FWHM duration is still in the attosecond range. Calculated bunch charge is 1.5 fC and average energy is 10 MeV.

FWHM duration, 0.2 mm away from the optical focus.

Finally, the transverse coherence length of the filtered bunch in Fig. 6 was calculated to be $L_T = 1.4 \times 10^{-2} \text{ nm}$. For a demonstration UED experiment, the electron pulse would then need to be focused to have a coherence length that is sufficiently long to form useful images; typically $L_T > 1 \text{ nm}$ is needed [20]. We emphasize that focusing is necessary to keep a maximum of the charges in the bunch. But this operation is likely to increase the bunch duration, as the net focusing effect of the current magnetic lenses used in UED beamlines depends on the electron energy. With focusing in mind, it is probably safer to say that the final electron pulse duration would be in the few-fs range.

5. Conclusion

Using three-dimensional particle-in-cell simulations, we have shown that relativistic electron pulses can be produced by focusing tightly few-cycle radially-polarized laser pulses in a low density atomic gas. In particular, we observed that for a laser power in the few-TW range, longitudinal attosecond microbunching occurs naturally, resulting in femtosecond structures with high-contrast attosecond density modulations.

It was demonstrated that in certain conditions the leading attosecond substructure survives to propagation over millimeter-scale distances. Combined with a high-pass energy filter and a focusing element, the proposed method could allow relativistic electron diffraction with a temporal resolution in the few-fs range, potentially sub-fs duration with a dispersion compensator.

Optimization of the laser pulse and gas parameters is currently being studied to improve the final bunch quality and total charge. Preferably, future work should include realistic modeling of the beamline to include the effects associated with the energy filter and focusing element. We emphasize that increasing the bunch charge is currently the most critical issue toward real application of the method.

Acknowledgments

This research was supported by the Natural Sciences and Engineering Research Council of Canada (NSERC). Computations were done on the supercomputer Briarée from Université de Montréal, managed by Calcul Québec and Compute Canada. The operation of this supercomputer is funded by the Canada Foundation for Innovation (CFI), NanoQuébec, RMGA and the Fonds de recherche du Québec - Nature et technologies (FRQ-NT). The authors gratefully acknowledge the EPOCH development team. The

EPOCH code used in this research was developed under UK Engineering and Physics Sciences Research Council grants EP/G054940/1, EP/G055165/1 and EP/G056803/1. CV thanks François Légaré and Martin Centurion for stimulating discussions.

- [1] Carbone F, Musumeci P, Luiten O and Hebert C 2012 *Chem. Phys.* **392** 1–9
- [2] Hada M, Pichugin K and Sciaini G 2013 *Eur. Phys. J. ST* **222** 1093–1123
- [3] Tokita S, Inoue S, Masuno S, Hashida M and Sakabe S 2009 *Appl. Phys. Lett.* **95** 111911
- [4] Uhliga J, Wahlströma C G, Walczaka M, Sundströma V and Fullagara W 2011 *Laser Part. Beams* **29** 415–425
- [5] Payeur S, Fourmaux S, Schmidt B E, MacLean J P, Tchervenkov C, Légaré F, Piché M and Kieffer J C 2012 *Appl. Phys. Lett.* **101** 041105
- [6] He Z H, Hou B, Nees J A, Easter J H, Faure J, Krushelnick K and Thomas A G R 2013 *New J. Phys.* **15** 053016
- [7] Breuer J and Hommelhoff P 2013 *Phys. Rev. Lett.* **111** 134803
- [8] Marceau V, Varin C, Brabec T and Piché M 2013 *Phys. Rev. Lett.* **111** 224801
- [9] Marceau V, Hogan-Lamarre P, Brabec T, Piché M and Varin C 2015 *J. Phys. B: At. Mol. Opt. Phys.* **48** 045601
- [10] Schlenvoigt H P, Haupt K, Debus A, Budde F, Jäckel O, Pfotenhauer S, Schwoerer H, Rohwer E, Gallacher J G, Brunetti E, Shanks R P, Wiggins S M and Jaroszynski D A 2007 *Nat. Phys.* **4** 130–133
- [11] Fuchs M, Weingartner R, Popp A, Major Z, Becker S, Osterhoff J, Cortrie I, Zeitler B, Hörlein R, Tsakiris G D, Schramm U, Rowlands-Rees T P, Hooker S M, Habs D, Krausz F, Karsch S and Grüner F 2009 *Nat. Phys.* **5** 826–829
- [12] Kneip S, McGuffey C, Martins J L, Martins S F, Bellei C, Chvykov V, Dollar F, Fonseca R, Huntington C, Kalintchenko G, Maksimchuk A, Mangles S P D, Matsuoka T, Nagel S R, Palmer C A J, Schreiber J, Phuoc K T, Thomas A G R, Yanovsky V, Silva L O, Krushelnick K and Najmudin Z 2010 *Nat. Phys.* **6** 980–983
- [13] Cipiccia S, Islam M R, Ersfeld B, Shanks R P, Brunetti E, Vieux G, Yang X, Issac R C, Wiggins S M, Welsh G H, Anania M P, Maneuski D, Montgomery R,

Smith G, Hoek M, Hamilton D J, Lemos N R C, Symes D, Rajeev P P, Shea V O, Dias J M and Jaroszynski D A 2011 *Nat. Phys.* **7** 867–871

[14] Hastings J B, Rudakov F M, Dowell D H, Schmerge J F, Cardoza J D, Castro J M, Gierman S M, Loos H and Weber P M 2006 *Appl. Phys. Lett.* **89** 184109

[15] Murooka Y, Naruse N, Sakakihara S, Ishimaru M, Yang J and Tanimura K 2011 *Appl. Phys. Lett.* **98** 251903

[16] Malka V 2012 *Phys. Plasmas* **19** 055501

[17] Hooker S M 2013 *Nat. Photonics* **7** 775–782

[18] Peralta E A, Soong K, England R J, Colby E R, Wu Z, Montazeri B, McGuinness C, McNeur J, Leedle K J, Walz D, Sozer E B, Cowan B, Schwartz B, Travish G and Byer R L 2013 *Nature* **503** 91–4

[19] England R J, Noble R J, Bane K, Dowell D H, Ng C K, Spencer J E, Tantawi S, Wu Z, Byer R L, Peralta E, Soong K, Chang C M, Montazeri B, Wolf S J, Cowan B, Dawson J, Gai W, Hommelhoff P, Huang Y C, Jing C, McGuinness C, Palmer R B, Naranjo B, Rosenzweig J, Travish G, Mizrahi A, Schachter L, Sears C, Werner G R and Yoder R B 2014 *Rev. Mod. Phys.* **86** 1337–1389

[20] Sciaimini G and Miller R J D 2011 *Rep. Prog. Phys.* **74** 096101

[21] Musumeci P, Moody J T, Scoby C M, Gutierrez M S and Westfall M 2010 *Appl. Phys. Lett.* **97** 063502

[22] Han J H 2011 *Phys. Rev. ST – Accel. Beams* **14** 050101

[23] Schmid K, Veisz L, Tavella F, Benavides S, Tautz R, Herrmann D, Buck A, Hidding B, Marcinkevicius A, Schramm U, Geissler M, Meyer-ter Vehn J, Habs D and Krausz F 2009 *Phys. Rev. Lett.* **102** 1–4

[24] Beaurepaire B, Lifschitz A and Faure J 2014 *New J. Phys.* **16** 023023

[25] Varin C and Piché M 2006 *Phys. Rev. E* **74** 2–5

[26] Karmakar A and Pukhov A 2007 *Las. Part. Beams* **25** 371–377

[27] Brady C S and Arber T D 2011 *Plasma Phys. Control. Fusion* **53** 015001

[28] Taflove A and Hagness S C 2005 *Computational Electrodynamics: The Finite-Difference Time-Domain Method* 3rd ed (Artech House)

[29] April A 2010 Ultrashort, strongly focused laser pulses in free space *Coherence and Ultrashort Pulse Laser Emission* ed Duarte F J (InTech) pp 355–382

[30] Marceau V, April A and Piché M 2012 *Opt. Lett.* **37** 2442–2444

[31] Rodríguez-Morales G and Chávez-Cerda S 2004 *Opt. Lett.* **29** 430–432

[32] Caron C F R and Potvliege R M 1999 *J. Mod. Opt.* **46** 1881–1891

[33] April A and Piché M 2010 *Opt. Express* **18** 22128–22140

[34] Lawrence-Douglas A 2013 *Ionisation Effects for Laser-Plasma Interactions by Particle-in-Cell Code* Ph.D. thesis University of Warwick

[35] Hartemann F V 2001 *High-Field Electrodynamics* (CRC Press)

[36] Varin C, Payeur S, Marceau V, Fourmaux S, April A, Schmidt B, Fortin P L, Thiré N, Brabec T, Légaré F, Kieffer J C and Piché M 2013 *Appl. Sci.* **3** 70–93

[37] Fortin P L, Piché M and Varin C 2010 *J. Phys. B: At. Mol. Opt. Phys.* **43** 025401

[38] Michalik A M and Sipe J E 2009 *J. Appl. Phys.* **105** 084913

[39] Siwick B J, Dwyer J R, Jordan R E and Miller R J D 2002 *J. Appl. Phys.* **92** 1643

[40] Tokita S, Hashida M, Inoue S, Nishioji T, Otani K and Sakabe S 2010 *Phys. Rev. Lett.* **105** 215004

[41] Hansen P, Baumgarten C, Batelaan H and Centurion M 2012 *Appl. Phys. Lett.* **101** 083501